The carbon ⟨100⟩ split interstitial in SiC

2002 J. Phys.: Condens. Matter 14 12433

(http://iopscience.iop.org/0953-8984/14/47/316)

INSTITUTE OF PHYSICS PUBLISHING JOURNAL OF PHYSICS: CONDENSED MATTER

J. Phys.: Condens. Matter **14** (2002) 12433–12440 PII: S0953-8984(02)39976-4

The carbon ⟨100⟩ split interstitial in SiC

T T Petrenko, T L Petrenko and V Ya Bratus'

Institute of Semiconductor Physics, NASU, 45 Prospect Nauky, 03028 Kyiv, Ukraine

E-mail: tarpetrenko@hotmail.com (T T Petrenko)

Received 25 July 2002
Published 15 November 2002
Online at stacks.iop.org/JPhysCM/14/12433

Abstract

A cluster calculation of hyperfine coupling constants based on density functional theory (DFT) has been performed for the carbon ⟨100⟩ split interstitial (V_C + 2C) in various charge and spin states in cubic SiC along with the dihydrogen-containing defect (V_C + 2H). Compared to the isolated carbon vacancy, the presence of two carbon atoms in the split interstitial centre causes lowering of the point symmetry for positive and negative charge states from D_{2d} to D_2 and substantially reduces the spin density on the nearest Si neighbours. The DFT-based approach has been used for a calculation of the zero-field splitting parameters D and E of the neutral $(V_C+2C)^0$ state with spin $S = 1$. Singly charged and neutral carbon ⟨100⟩ split interstitial defects are suggested as a microscopic model of the well-known T5 (initially identified as V_C^+ and then re-identified as a dihydrogen-containing complex) and EI3 centres in SiC, respectively.

1. Introduction

Silicon carbide is an attractive semiconductor material for electronic applications owing to the high saturated drift velocity and high breakdown field, high thermal and chemical stability and feasibility of use in extreme environments. Continuing progress in bulk and epitaxial growth of SiC and device processing technology [1] calls for a reasonably accurate picture of intrinsic and irradiation-induced defects. Among various experimental techniques, the electron paramagnetic resonance (EPR) and electron–nuclear double-resonance (ENDOR) approaches are the most suitable tools for obtaining a deep insight into the microscopic structure of defects. The native defects in various polytypes of SiC have been the subject of a great number of EPR studies in the last few years. In principle, close inspection of the hyperfine structure of the EPR spectra makes it possible to suggest a tentative microscopic model of a defect. However, the final verification of the adequacy of the model needs additional experimental and theoretical arguments. For example, of the numerous point defects created by irradiation of SiC and observed by means of EPR, there are a lot of centres with spin $S = 1$ and inherent zero-field splitting (ZFS) varying over a wide range. They have been tentatively

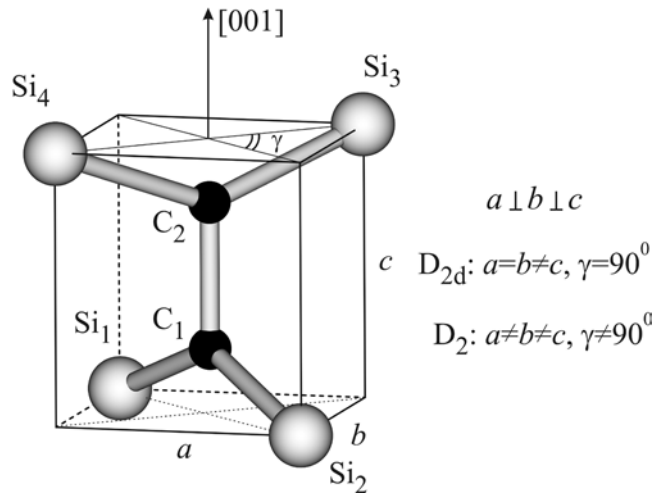

Figure 1. A model of the carbon ⟨100⟩ split interstitial in cubic SiC, where the C–C dumb-bell occupies a carbon substitutional site. The D_{2d} symmetry corresponds to the neutral charge state of the defect, while it reduces to D_2 for the singly charged states.

assigned to both isolated [2] and paired defects [3, 4]. To our knowledge, none of these defects has been unambiguously identified. Overall, among the vacancies, interstitials, antisites and Frenkel pairs appearing as the simplest forms of defects in silicon carbide, the former are best understood [4–6].

Over the past few years, considerable advances have been made in the field of first-principles calculations of intrinsic defects in SiC (see, for example, [6] and references therein). Specifically, calculations of the formation energies and properties of vacancies in SiC provide great support for the proposed defect models [7–12]. Calculations of the point symmetry, ground spin state and hyperfine parameters (HFPs) of a defect provide an opportunity for making a direct comparison with the EPR data [11, 12]. Applying them, the microscopic structure of the silicon vacancy in the negative (V_{Si}^{-}) charge state [7–10] and that of the carbon vacancy in the positive (V_{C}^{+}) charge state [12–14] have been reliably identified. The identification of the other intrinsic defects in silicon carbide is still a problem of vital importance.

In contrast to the cases for silicon and diamond, an isolated interstitial has not so far been found by means of EPR in SiC. According to semi-empirical molecular orbital (MO) calculations for the diamond lattice [15], the ⟨100⟩ split interstitial has significantly lower formation energy than interstitials in tetrahedral, hexagonal and bond-centred sites. The configuration of this defect corresponds to a ⟨100⟩-directed Si–Si, Si–C or C–C dumb-bell centred on a substitutional site (figure 1). In diamond, the neutral carbon ⟨100⟩ split interstitial [16] as well as the di-⟨100⟩ split interstitial [17] have already been identified. In silicon, an EPR spectrum labelled as Si-G12 has been identified as arising from a ⟨100⟩ C–Si split interstitial [18]. Contrastingly, the Si-G11 spectrum has been identified as that of the Jahn–Teller-distorted ⟨111⟩ C–C split interstitial [19]. As has been recently shown [6, 20], the carbon ⟨100⟩ split interstitial possesses the lowest formation energy after the carbon vacancy among carbon-related defects in cubic SiC. It can exist in the charge states of +2, +1, 0 and −1 as the Fermi-level position changes from the valence band maximum to the conduction band minimum, while its formation energy ranges from 5.5 to 7.5 eV [20]. For most of the listed charge states, this defect is paramagnetic and could be observed by means of EPR.

It is appropriate to mention the T5 centre [4, 21], whose structure is furiously debated. Observed only after irradiation of epitaxially grown p-type cubic SiC, this carbon-site-related defect has D_2 symmetry, spin $S = 1/2$ and the principal axes of the g-tensor are found to be along the ⟨100⟩ directions; its tensor of hyperfine interaction is approximately axially symmetric along the ⟨111⟩ axes. On the basis of the intensity ratio of all hyperfine lines to the Zeeman lines, the T5 centre was originally identified as a V_C^+ defect in 3C-SiC. Subsequent theoretical and experimental studies of the carbon vacancy in SiC called this identification into question. It has been shown by first-principles calculation [8, 12] that, similarly to the positively charged vacancy in Si [22], the Jahn–Teller distortion lowers the symmetry of V_C^+ in 3C-SiC to D_{2d}. In hexagonal 4H and 6H polytypes of SiC, some carbon vacancy-related defects with HFPs about three times those for the T5 centre have been recently attributed to V_C^+ [14, 23]. The adequacy of this assignment has been proved with theoretical simulation of HFPs for the nearest-neighbour (NN) and next-nearest-neighbour (NNN) atoms of V_C^+ in SiC [11, 12]. Recently, a revised assignment of the T5 centre as the dihydrogen $(V_C + 2H)^+$ complex has been proposed [24]. Notice that carbon vacancy-related defects with hyperfine splittings similar to those of the T5 centre have been found with spin $S = 1/2$ (EI1 centre) and $S = 1$ (EI3 centre) in 4H- and 6H-SiC [25].

In this paper, the results of calculations based on density functional theory (DFT) of hyperfine and zero-field-splitting parameters of the carbon ⟨100⟩ split interstitial, designated hereafter as $(V_C + 2C)$, in various charge states are presented. The hyperfine interaction with protons and the four nearest ^{29}Si nuclei is also examined for the $(V_C + 2H)$ model. On the basis of calculations, reassignments of the T5 and EI3 centres are proposed.

2. Method of calculations

Cluster DFT calculations of HFPs were performed for atoms of the first and second shells of a defect as well as for two central carbons or hydrogens involved in its structure. The $C_2Si_{16}C_{18}H_{36}$ and $H_2Si_{16}C_{18}H_{36}$ tetrahedral clusters were used, whose size gives a reasonable compromise between the accuracy of the calculated HFPs and the CPU time [12]. Calculations were performed using the Gaussian 94W and Gaussian 98 packages [26]. Becke's three-parameter hybrid exchange–correlation functional (B3LYP) [27] was used, including gradient corrections (see, for example, [28] and references therein). All atoms of a cluster were allowed to relax during the total energy minimization, with the exception of the capped bond hydrogen atoms that were at fixed positions.

Two types of Gaussian basis set were used to reproduce the spin density at the centre of a cluster adequately. The first type, designated as I in table 1, implies an EPR-III basis for two central carbons, 6-311G(d) for the NN Si atoms together with a 6-31G(d) basis set for the other atoms of a cluster. The second type (II) implies a 6-311G(d, p) basis for two central hydrogens, a 6-311G(d) one for the NN Si atoms and 6-31G(d) for other atoms. In both cases we used the STO-3G basis set for the capped bond hydrogens. The double-ζ basis set EPR-II and the triple-ζ set EPR-III were found particularly appropriate for calculations of the Fermi contact term [29].

The isotropic hyperfine coupling constant a_{iso} and the components T_{ij} of the traceless tensor of the anisotropic hyperfine interaction were calculated according to the standard first-order relations [12]. The accuracy of the approaches used for the calculations of the HFPs was examined for V_{Si}^- and V_C^+ in SiC together with V_{Si}^+ in silicon and a good coincidence with experimental values was obtained [10–12].

For the defects with spin $S \geqslant 1$ and low point symmetry, the zero-field splitting is of importance. To our knowledge, the validity of DFT-based calculations for reproduction of the

Table 1. The point symmetry and optimized atomic geometry (see figure 1) of the carbon ⟨100⟩ split interstitial in various charge states.

Defect, charge state	Point symmetry	a (Å)	b (Å)	c (Å)	C_1–C_2 distance (Å)
$(V_C + 2C)^+$	D_2	2.359	2.483	2.603	1.297
$(V_C + 2C)^0$	D_{2d}	2.352	2.352	2.572	1.376
$(V_C + 2C)^-$	D_2	2.238	2.361	2.548	1.403

observed ZFS parameters D and E has not been tested up to now. In the general case, the ZFS originates from both spin–spin and spin–orbit interactions. The former dominates for the compounds containing elements of the first and second rows, e.g. for CH_2, while for heavier elements the spin–orbit contribution can be more significant, as in the case of SiH_2 [30]. As will be shown later, for neutral carbon ⟨100⟩ split interstitial $(V_C + 2C)^0$ in triplet spin state, the spin density is localized mainly on two carbon atoms that form a ⟨100⟩-oriented C–C dumb-bell. Thus, it is reasonable in this case to expect the main contribution to the ZFS to be caused by spin–spin interaction.

The general expression for the elements of the spin–spin coupling tensor was obtained in [31] using the appropriate term in the Breit–Pauli Hamiltonian:

$$D_{pq} = \frac{1}{4}g^2\beta^2 \iint \frac{1}{(r_{12})^5}[(r_{12})^2\delta_{pq} - 3(x_{12})_p(x_{12})_q]Q_{ca}(r_1, r_2)\,\mathrm{d}r_1\,\mathrm{d}r_2 \quad (1)$$

where $\boldsymbol{r}_{12} = \boldsymbol{r}_1 - \boldsymbol{r}_2$ and Q_{ca} is 'the coupling anisotropy function' [31] or, in terms of [32], the 'spin correlation function'.

In the case of the single-determinant wavefunction with all spin orbitals being mutually orthogonal, the function Q_{ca} can be expressed in terms of the spin density matrix Q_{ij} and basis functions ϕ_i [31]:

$$D_{pq} = \frac{g^2\beta^2}{4S(2S-1)}\sum_{ijkl}(Q_{ij}Q_{kl} - Q_{kj}Q_{il}) \times \langle\phi_j(1)\phi_l(2)|\frac{(r_{12})^2\delta_{pq} - 3(x_{12})_p(x_{12})_q}{(r_{12})^5}|\phi_i(1)\phi_k(2)\rangle \quad (2)$$

where indices $ijkl$ run over all basis functions of the cluster considered.

The widely used point dipole and 'two-electrons-in-two-orbitals' approximations are particular cases of relationship (2). As distinct from the latter approach used for the carbon split interstitial in diamond [33], the expression (2) takes into account the all-electron contribution and the effects of spin polarization. Spectroscopic parameters D and E can be expressed in terms of principal values of the matrix D_{pq} as $D = -(3/2)D^0_{zz}$ and $E = -(1/2)(D^0_{xx} - D^0_{yy})$. The choice of principal directions is made similarly to that in [30], to make $|D| \geqslant |3E|$ and $DE < 0$.

To examine the performance of this DFT-based approach to the calculation of 'spin–spin-only' ZFS parameters, we have made a calculation for carbene CH_2 in the triplet spin state. According to estimates [30], in this case, the spin–orbit contributions $D_{SO} = 0.023$ cm^{-1} and $E_{SO} = 0.0001$ cm^{-1} are negligible as compared with the experimental values $|D_{exp}| = 0.7567$ cm^{-1} and $|E_{exp}| = 0.0461$ cm^{-1}. Thus, the triplet carbene is appropriate for use in a test calculation of 'spin–spin-only' ZFS parameters. At the B3LYP level of theory with the EPR-II basis for carbon and EPR-III for hydrogen atoms, the values calculated according to equation (2) are equal to $D = 0.897$ cm^{-1} and $E = -0.052$ cm^{-1} for triplet-optimized geometry. For the linear CH_2 configuration the calculations give $D = 1.042$ cm^{-1} and

Table 2. Calculated HFPs for carbon ⟨100⟩ split interstitials and dihydrogen defects in various charge states in cubic SiC. The atoms labelled Si_1–Si_4 are the nearest neighbours of two central carbons (C_1, C_2) (figure 1) or hydrogens (H_1, H_2).

Defect, charge and spin state	Point symmetry, basis set	Atoms	Hyperfine coupling parameters (in 10^{-4} cm^{-1})			
			a_{iso}	T_{11}	T_{22}	T_{33}
$(V_C + 2C)^+$	D_2	Si_1–Si_4	−12.4	−3.6	1.7	1.9
$S = 1/2$	I	C_1, C_2	5.9	27.5	−12.3	−15.2
$(V_C + 2C)^-$	D_2	Si_1–Si_4	−14.9	−3.2	1.4	1.8
$S = 1/2$	I	C_1, C_2	6.0	23.6	−11.8	−11.8
$(V_C + 2C)^0$	D_{2d}	Si_1–Si_4	−13.0	−3.1	1.4	1.7
$S = 1$	I	C_1, C_2	6.0	−12.2	18.7	−6.5
$(V_C + 2H)^+$	D_2	Si_1–Si_4	−40.0	−16.3	7.9	8.4
$S = 1/2$	II	H_1, H_2	−16.6	9.6	−5.2	−4.4
$(V_C + 2H)^{3+}$	D_{2d}	Si_1–Si_4	6.8	−3.5	1.7	1.8
$S = 1/2$	II	H_1, H_2	25.2	0.5	−0.2	−0.3
$(V_C + 2H)^-$	D_2	Si_1–Si_4	−64.5	−15.3	7.0	8.3
$S = 1/2$	II	H_1, H_2	−13.6	2.07	−0.94	−1.13
V_C^+	D_{2d}	Si_1–Si_4	−40.9	−15.3	6.8	8.5
$S = 1/2$ [8]	I					
T5 [17]	D_2	Si_1–Si_4	±15.5	±3.4	∓1.7	∓1.7

$E = 0$. Thus, the agreement with experiment is quite good, though somewhat inferior to results obtained with higher level methods [30].

3. Results and discussion

The results of calculations of the point symmetry and optimized geometry of the carbon ⟨100⟩ split interstitial in various charge and related ground spin states are presented in table 1. The HFPs of the defects under examination are exhibited in table 2 along with the theoretically estimated parameters for V_C^+ [12] and experimental EPR data for the T5 centre [21]. Relative to the isolated V_C^+ defect, carbon ⟨100⟩ split interstitial formation substantially reduces the spin density on the nearest Si neighbours. A close coincidence of the point symmetry and HFPs is revealed for both positive and negative charge states of the (V_C + 2C) defect and experimental values for the T5 centre. In any case, 'T5-like' hyperfine splittings are expected for both charge states of the (V_C + 2C) defect. Arguments mentioned in [4] and [21] give grounds for considering the T5 centre as a positively charged defect in irradiated p-type 3C-SiC. Though the position of the ionization level (−/0) calculated for V_{Si}^- in [8, 20] and the defect formation energies calculated for various charge states of carbon split interstitials in [20] show that the possibility of negative charge of the T5 centre cannot be excluded, positive charge is more probable. The splitting caused by hyperfine interaction with ^{13}C (having nuclear spin $I = 1/2$ and natural abundance $\rho = 1.11\%$) could be expected but hidden under dominant ^{29}Si ($I = 1/2$, $\rho = 4.71\%$) hyperfine lines in a sample of SiC not enriched with ^{13}C.

The nearly equal values of the calculated HFPs for all charge states of carbon ⟨100⟩ split interstitials under consideration is a rather significant result. In order to gain some insight into this effect, we performed an auxiliary calculation for $(V_C + 2C)^{2+}$, which revealed the D_{2d} point symmetry of this defect. For charge states $Q = +1$, 0 and −1 the additional k electrons ($k = 1$, 2 and 3, respectively) fill two virtual bonding MOs of the e type. For $k = 1$ and 3 the

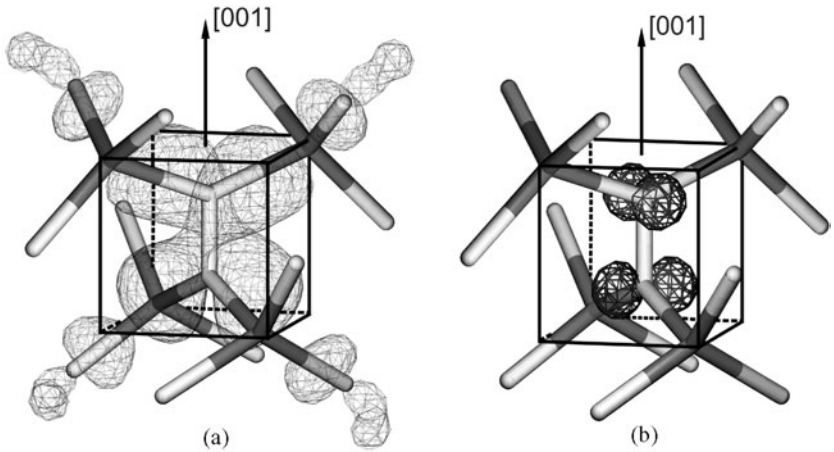

Figure 2. A schematic picture of carbon ⟨100⟩ split interstitials in SiC and MOs which determine the symmetry and paramagnetic properties of this defect. The shading scheme used is: dark grey for silicon and light grey for carbon. (a) The isosurface of the absolute value of the highest occupied MO for the positively charged defect, corresponding to 4% of its maximum magnitude. (b) Localized MOs occupied by two α-electrons for a neutral charge state with spin $S = 1$. This isosurface corresponds to 20% of its maximum magnitude.

charge density corresponding to such extra orbitals is of D_2 symmetry, while for $k = 2$ it is of D_{2d} symmetry. Thus, for $Q = \pm 1$ the Jahn–Teller distortion occurs from D_{2d} to D_2. For all the charge states examined, the bonding MOs occupied with unpaired electrons make the dominant contribution to the spin density distribution (see figure 2(a)) and appear to be slightly varied, depending on Q. This is reflected in the pronounced similarity of the HFPs for central carbon and NN Si atoms in different charge states.

The electron density corresponding to bonding MOs is formed mainly by p_x and p_y orbitals of the central C atoms (if the z-axis is chosen parallel to C–C bond). Thus, the density constituting the additional C–C bonding for the carbon split interstitial concentrates mainly beyond the C–C axis. This feature is inherent to π-bonding systems.

It is known that in irradiated diamond the neutral charge state of the carbon split interstitial labelled as the R2 centre is EPR active with spin $S = 1$ [16]. Calculations show that singlet and triplet states are rather close in energy in this case [33]. Our calculations for cubic SiC gave the total energy gain of 0.540 eV for the triplet state as compared to the singlet one. Similar behaviour is expected for hexagonal polytypes.

A comparison of calculated spectroscopic parameters for the $(V_C + 2C)^0$ defect with those of the EI3 centre [25] reveals a lot of similarities. Since only the EPR spectrum for $\vec{H} \parallel \vec{c}$ is presented in [25], hyperfine splittings have been estimated for this orientation using HFPs from the table 2. For the nearest ^{29}Si atoms the calculated splittings in the EPR spectrum are 17.2, 13.1 and 12.8 G (double intensity), which are closely related to the values 19.2, 16.8 and 12.5 G (double intensity) observed for 4H-SiC [25]. The isotropic hyperfine splitting of about 3.9 G was attributed in [25] to the interaction with ^{13}C in the NNN shell. Our calculations revealed that among twelve NNN carbon sites, four of them give small splittings hidden under the intense central line. The other eight NNN carbon sites exhibit nearly isotropic hyperfine splittings in the range from 4.75 to 6.48 G for $\vec{H} \parallel \langle 111 \rangle$. In addition, two hyperfine doublets of 3.8 and 21.9 G originating from two central carbon atoms C_1 and C_2 should be observed in this orientation. The first doublet is hidden under the other lines of the EPR spectrum. The

second one is well resolved; however, it has very low intensity: about 0.55% of that of the central line.

Another essential feature of the EPR spectrum inherent to the EI3 centre is a relatively large value of the ZFS parameter D. Closely related values of 0.0552 and 0.0559 cm^{-1} have been found for 4H- and 6H-SiC, respectively [25]. To elucidate qualitatively the nature of the ZFS in the framework of the carbon split interstitial model, we have performed a transformation of the Kohn–Sham delocalized orbitals into a set of localized ones using the Boys method [34]. As a result, two α-electrons localized on atomic p orbitals of C_1 or C_2 atoms have been obtained (see figure 2(b)). The other localized orbitals may be approximately regarded as normal two-centre two-electron chemical bonds that do not contribute to the ZFS. Using the point dipole approximation, an estimation of the ZFS parameter D according to the relation $D = (3/2)g^2\beta^2/R^3$, where R is the C_1–C_2 distance, gives a value that is 12 times the experimental one. Notice that for the related R2 centre in diamond, the point dipole approximation is also inappropriate and gives a value of D that is 8 times that from the experiment [33]. At the same time, the 'two-electrons-in-two-orbitals' model for the R2 centre, taking into account the effects of delocalization, gives much better agreement for the ZFS parameter D [33]. To obtain a more reliable estimation of D in the case of SiC, we performed calculations of ZFS parameters according to equation (2)—however, using the smaller cluster $C_2Si_4H_{12}$ due to the extended CPU time. The validity of such calculations for the smaller cluster is supported by the fact that for both 72- and 18-atom clusters the spin density concentrated mainly on the central C_1 and C_2 atoms is reproduced nearly identically. In support of this statement, the values of HFPs for these atoms calculated with the smaller cluster, $a_{iso} = 5.96 \times 10^{-4}$ cm^{-1}, $T_{11} = -12.24 \times 10^{-4}$ cm^{-1}, $T_{22} = 20.16 \times 10^{-4}$ cm^{-1}, $T_{33} = -7.92 \times 10^{-4}$ cm^{-1}, are close to the values for the larger one presented in table 2. Also, the distances between the C_1 and C_2 atoms in the two clusters differ by only 0.013 Å. Using this procedure, we obtain $D = 0.067$ cm^{-1} and $E = 0$ in reasonable agreement with the experiment ($D_{exp} \approx 0.056$ cm^{-1}). The principal axis of the D-tensor makes an angle of 54.5° with the ⟨111⟩ direction in cluster versus 46° with the c-axis in 4H- and 6H-SiC [25]. Thus, these T5 and EI3 centres may be regarded as the same defect in the various charge states. An additional argument in favour of this statement is that the two centres show similar annealing behaviour [21, 25].

The results presented in table 2 demonstrate that the (V_C+2H) model for the T5 centre [24] exhibits a considerable discrepancy with experiment. On the one hand, the HFPs with the NN silicon atoms substantially differ from the experimental values. On the other, the (V_C + 2H) defect in the paramagnetic state should manifest a well-resolved doublet splitting due to hyperfine interaction with protons—in contrast with EPR data for the T5 centre. It should be remarked that for these centres we have also found a number of minima with somewhat higher total energies similar to those in [24]. However, the HFPs with hydrogens are likewise sufficiently large.

In summary, on the basis of a DFT-based calculation of the point symmetry and HFPs, the singly charged and neutral carbon ⟨100⟩ split interstitial are suggested as microscopic models of T5 and EI3 centres, respectively. Two carbon atoms manifest themselves only through the sufficient decrease of the spin density on nearest Si atoms as compared to V_C^+, while the major part of the spin density is localized on two central carbons. Their presence causes lowering of the point symmetry from D_{2d} for V_C^+ to D_2 for the singly charged carbon ⟨100⟩ split interstitial defect. In the neutral charge state, the interaction of two spins localized on central carbons accounts for the large zero-field splitting. We hope that our calculations of carbon split interstitial properties will prompt further experimental work on defects of this type in SiC.

Acknowledgments

This work was partially supported by French–Ukrainian project 9350. The calculations were carried out with the computational resources of the Calculation Centre CCR at Jussieu and the Information Computer Centre of National Taras Shevchenko University of Kyiv, which was established by the Intel Corporation.

References

[1] Harris G L (ed) 1995 *Properties of Silicon Carbide* (London: INSPEC)
[2] von Bardeleben H J, Cantin J L and Vickridge I 2000 *Phys. Rev.* B **62** 10126
[3] Son N T, Hai P N and Janzén E 2001 *Mater. Sci. Forum* **353–356** 499
[4] Itoh H, Kawasuso A, Ohshima T, Yoshikawa M, Nashiyama I, Tanigawa S, Misawa S, Okumura H and Yoshida S 1997 *Phys. Status Solidi* a **162** 173
[5] Bratus' V Ya, Petrenko T T, von Bardeleben H J, Kalinina E V and Hallén A 2001 *Appl. Surf. Sci.* **184** 229
[6] Bockstedte M, Heid M, Mattausch A and Pankratov O 2002 *Mater. Sci. Forum* **389–393** 471
[7] Wimbauer T, Meyer B K, Hofstaetter A, Scharmann A and Overhof H 1997 *Phys. Rev.* B **56** 7384
[8] Zywietz A, Furthmüller J and Bechstedt F 1999 *Phys. Rev.* B **59** 15166
[9] Torpo L, Nieminen R M, Laasonen K E and Pöykkö S 1999 *Appl. Phys. Lett.* **74** 221
[10] Petrenko T T, Petrenko T L and Bratus' V Ya 2002 *Phys. Solid State* **44** 831
[11] Petrenko T T, Petrenko T L, Bratus' V Ya and Monge J L 2001 *Appl. Surf. Sci.* **184** 273
[12] Petrenko T T, Petrenko T L, Bratus V Ya and Monge J L 2001 *Physica* B **308–310** 637
[13] Bratus' V Ya, Makeeva I N, Okulov S M, Petrenko T L, Petrenko T T and von Bardeleben H J 2001 *Mater. Sci. Forum* **353–356** 517
[14] Bratus V Ya, Makeeva I N, Okulov S M, Petrenko T L, Petrenko T T and von Bardeleben H J 2001 *Physica* B **308–310** 621
[15] Mainwood A, Larkins F P and Stoneham A M 1978 *Solid-State Electron.* **21** 1431
[16] Hunt D C, Twitchen D J, Newton M E, Baker J M, Anthony T R, Banholzer W F and Vagarali S S 2000 *Phys. Rev.* B **61** 3863
[17] Twitchen D J, Newton M E, Baker J M, Tucker O D, Anthony T R and Banholzer W F 1996 *Phys. Rev.* B **54** 6988
[18] Watkins G D and Brower K L 1976 *Phys. Rev. Lett.* **36** 1329
[19] Brower K L 1974 *Phys. Rev.* B **9** 2607
[20] Mattausch A, Bockstedte M and Pankratov O 2001 *Mater. Sci. Forum* **353–356** 323
[21] Itoh H, Yoshikawa M, Nashiyama I, Misawa S, Okumura H and Yoshida S 1992 *J. Electron. Mater.* **21** 707
[22] Watkins G 1965 *Radiation Damage in Semiconductors* (Paris: Dunod) p 97
[23] Son N T, Hai P N and Janzén E 2001 *Phys. Rev.* B **63** 201201(R)
[24] Aradi B, Gali A, Deák P, Lowther J E, Son N T, Janzén E and Choyke W J 2001 *Phys. Rev.* B **63** 245202
[25] Son N T, Chen W M, Lindström J L, Monemar B and Janzén E 1999 *Mater. Sci. Eng.* B **61/62** 202
[26] Frisch M J, Trucks G W, Schlegel H B, Scuseria G E, Robb M A, Cheeseman J R, Zakrzewski V G, Montgomery J A Jr, Stratmann R E, Burant J C, Dapprich S, Millam J M, Daniels A D, Kudin K N, Strain M C, Farkas O, Tomasi J, Barone V, Cossi M, Cammi R, Mennucci B, Pomelli C, Adamo C, Clifford S, Ochterski J, Petersson G A, Ayala P Y, Cui Q, Morokuma K, Malick D K, Rabuck A D, Raghavachari K, Foresman J B, Cioslowski J, Ortiz J V, Baboul A G, Stefanov B B, Liu G, Liashenko A, Piskorz P, Komaromi I, Gomperts R, Martin R L, Fox D J, Keith T, Al-Laham M A, Peng C Y, Nanayakkara A, Gonzalez C, Challacombe M P, Gill P M W, Johnson B, Chen W, Wong M W, Andres J L, Gonzalez C, Head-Gordon M, Replogle E S and Pople J A 1998 *Gaussian 98, Revision A.7* (Pittsburgh, PA: Gaussian)
[27] Becke A D 1993 *J. Chem. Phys.* **98** 5648
[28] Barone V 1994 *J. Chem. Phys.* **101** 6834
[29] Barone V 1995 *Recent Advances in Density Functional Methods* ed D P Chong (Singapore: World Scientific)
[30] Havlas Z, Downing J W and Michl J 1998 *J. Phys. Chem.* A **102** 5681
[31] McWeeny R and Mizuno Y 1961 *Proc. R. Soc.* A **259** 554
[32] McLachlan A D 1963 *Mol. Phys.* **6** 441
[33] Goss J P, Coomer B J, Jones R, Shaw T D, Briddon P R, Rayson M and Öberg S 2001 *Phys. Rev.* B **63** 195208
[34] Boys S F 1960 *Rev. Mod. Phys.* **32** 296